Available online at www.sciencedirect.com
SCIENCE DIRECT®
Sensors and Actuators B 91 (2003) 241–251
SENSORS AND ACTUATORS B CHEMICAL
www.elsevier.com/locate/sensorb

Label-free highly sensitive detection of (small) molecules by wavelength interrogation of integrated optical chips

K. Cottier[a,*], M. Wiki[b], G. Voirin[a], H. Gao[a], R.E. Kunz[a]

[a]Centre Suisse d'Electronique et de Microtechnique SA (CSEM), Jaquet-Droz 1, CH-2007 Neuchâtel, Switzerland
[b]Unaxis Optics Ltd., P.O. Box 1000, FL-9496 Balzers, Liechtenstein

Abstract

A bio-chemical sensor system based on wavelength interrogation of integrated optical sensor chips is presented. The combination of a non-mechanical scanning approach with sensor chips of high quality and stability allows fast and accurate multi-channel measurements. The emphasis of the present paper lies in presenting detailed design considerations, and in reporting the application of the system to several high sensitivity sensing tasks.

An excellent performance of the sensor is demonstrated for bulk refractometry and affinity measurements. The bulk refractometric measurements show a detection limit of $<10^{-6}$. For detecting small molecules, a standard deviation in terms of mass coverage of 100 fg/mm^2 is obtained, corresponding to a detection limit of 0.3 pg/mm^2. Furthermore, a very clear signal is observed for biotin (244 Da), indicating a detection limit for the present wavelength interrogated optical sensor (WIOS) system distinctly below 200 Da. For a direct immunoassay at low concentrations, a detection limit in the order of 10^{-11} M is estimated based on the experimental results. The results show that the sensor is perfectly suited for application areas such as medical, food and environmental.

Keywords: Label-free sensing; (Bio-)chemical sensors; Evanescent-wave sensors; Integrated optical sensor chip

1. Introduction

Label-free detection of several analyte molecules being simultaneously present in a liquid or in a gas with high sensitivity is a major requirement for present and future applications of (bio-)chemical sensors, especially for areas such as medical, food and environmental. In this paper, newest results are reported that have been achieved by reading the signal of multiple sensing pads on an integrated optical (IO) chip simultaneously by a tunable laser [1]. Other approaches for label-free sensing making use of dielectric waveguides include optical waveguide lightmode spectroscopy (OWLS) [2,3], chirped grating couplers [4], Mach-Zehnder [5] and Young interferometers [6,7]. Other well-known methods are based on surface plasmon resonance (SPR) [8], resonant mirror [9], reflectometric interference spectroscopy (RifS) [10], scanning angle reflectometry (SAR) [11], surface acoustic waves (SAW) [12], quartz crystal microbalance [13] and fully electrical devices.

The main advantages of the approach presented in this paper are high sensitivity, fast response, small size and low cost. With the use of sensor chips on glass instead of polymer substrates [14], the stability and reproducibility of the measurements increased markedly.

In this paper, the theoretical fundamentals are presented, followed by a description of the sensing principle and the optical scheme. Then, design considerations as well as a detailed description of effects distorting the signal shape and the corresponding calibration possibilities are given. Next, the practical realization of the readout instrument and the measurement procedure are presented. After that, the fabrication of the chips is explained. Finally, experimental results for the application of the system to refractometry, detection of small molecules and low concentrations are reported.

2. Wavelength interrogation method

2.1. Theoretical fundamentals

2.1.1. Waveguide

A planar dielectric multi-layer waveguide is shown in Fig. 1. All layers are supposed to be absorption free and

* Corresponding author. Tel.: +41-32-720-51-79; fax: +41-32-720-57-40.
E-mail address: kaspar.cottier@csem.ch (K. Cottier).

0925-4005/03/$ – see front matter © 2003 Elsevier Science B.V. All rights reserved.
doi:10.1016/S0925-4005(03)00117-5

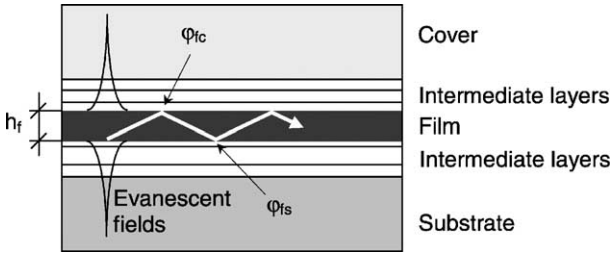

Fig. 1. Multi-layer waveguide.

without scattering. The mode propagates through total internal reflection inside the layer with the highest index of refraction, the so-called film. If the index of refraction decreases to the outer side of the system—such as no secondary waveguides are created—the guided modes fulfill the mode equation:

$$2kh_f\sqrt{n_f^2 - N^2} + \varphi_{fc} + \varphi_{fs} = 2\pi m \tag{1}$$

where h_f is the film height, n_f the film refractive index, N the effective refractive index of the waveguide, k the wave number, φ_{fc} the Fresnel reflection phase shift at top film interface, φ_{fs} the Fresnel reflection phase shift at bottom film interface and m the mode number.

In the case of a monomode waveguide, the right side of the equation reduces to zero.

The waveguide's effective refractive index N is directly proportional to the propagation constant of the mode. It is polarization dependent, as the Fresnel reflection phase shifts φ_{fc} and φ_{fs} differ for TE and TM waves.

In principle, the model only applies to unstructured interfaces. It can be used as an approximation to structured surfaces such as gratings when the grating depth h_g is small compared to the film thickness h_f. In this 'thin grating' approximation, the film height h_f does not correspond to the physical film thickness and is referred to as equivalent height. The model can be nevertheless expanded for structured interfaces by introducing additional layers with an averaged index of refraction [15].

2.1.2. Grating coupler

Light can be coupled into or out of a waveguide by means of a grating. A plane wave incident on the grating is partially diffracted into the guided mode. Maximum coupling efficiency is achieved at the resonance condition

$$n_a \sin\theta_{in} = N - \frac{m_g\lambda_r}{\Lambda} \tag{2}$$

where n_a is the ambient medium in which θ is measured, θ_{in} the angle of incidence of the plane wave, m_g the diffraction order, λ_r the resonance wavelength in the ambient medium and Λ the grating period.

2.1.3. Waveguide and grating of finite length

Both the models for waveguide and grating assume structures of infinite extent in the direction of propagation of the mode. A finite structure shows broadened resonances instead of discrete modes and coupling conditions. While the point of maximum coupling can be determined by Eqs. (1) and (2), width and shape of the resonance curve have to be determined with other models.

The effective index spread ΔN corresponding to a finite structure is derived in [16], Eq. (21):

$$\Delta N = \frac{\lambda}{L_g} \tag{3}$$

where L_g is the effective grating length.

The wavelength spread $\Delta\lambda$ in the case of a wavelength scan is given by:

$$\Delta\lambda = \Delta N\left(\frac{dN}{d\lambda}\right)^{-1} = \frac{\lambda}{L}\left(\frac{dN}{d\lambda}\right)^{-1} \tag{4}$$

where $dN/d\lambda$ is the effective index dispersion, given in [17].

The shape of the resonance curve $\eta = f(\lambda)$ of a finite grating can be approximated by a Lorentzian of center λ_r and halfwidth $\Delta\lambda/2$ [18].

2.2. Sensing principle

The wavelength interrogated optical sensor (WIOS) approach is based on scanning the resonance peak of a grating coupler by means of a current tunable laser diode.

The sensor chip is based on a monomode waveguide that is structured with two corrugated grating regions. The first one acts as incoupling pad for the incident beam, and the second grating for coupling light out of the waveguide onto a detector. When a guided mode is excited inside the waveguide, its evanescent field penetrates into the layers adjacent to the film. Changes of the optical properties in this region affect the phase shift φ_{fc} upon Fresnel reflection. The effective refractive index N of the waveguide mode changes accordingly (cf. Eq. (1)). The change in effective refractive index is monitored by observing the resonance peak of the incoupling grating (Eq. (2)).

In a classical readout scheme for a bio-chemical sensor based on waveguides and gratings, the resonance angle is scanned with a laser source of fixed wavelength [3]. In the wavelength interrogation approach, the resonance is scanned by observing the resonance wavelength at a fixed angle of incidence.

The sensing principle applies to two measurement configurations, namely (a) bulk refractive index sensing (refractive index of the cover medium n_c, Fig. 2a) and (b) measuring thickness h_l and/or refractive index n_l changes of a (bio-chemical) adlayer at the waveguide surface (Fig. 2b). Knowing the waveguide parameters, the measurand can be calculated from the relations (1) and (2).

The limited wavelength tuning range of the laser source results in a limited measurement range, tight fabrication

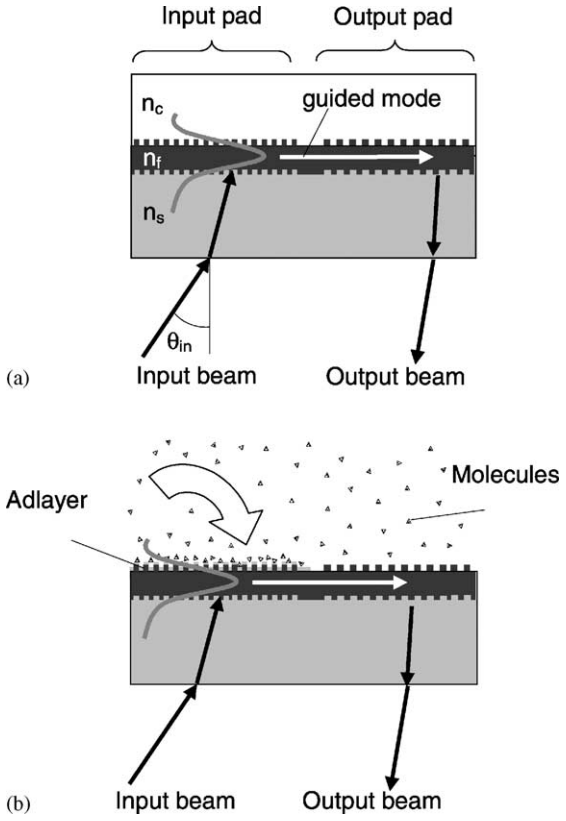

Fig. 2. (a) Bulk refractive index sensing. (b) Bio-chemical adlayer sensing.

tolerances for the sensor chips, and severe stabilization criteria. To overcome these limitations, an additional degree of freedom is introduced by adjusting the angle of incidence. Using a motorized mirror construction to set the working point introduces also the advantage of being able to perform an in situ chip calibration as described in Section 4.4

2.3. Optical scheme

The optical scheme is depicted in Fig. 3. A vertical cavity surface emitting laser diode (VCSEL) with a saw-tooth wavelength modulation is used as laser source. The collimated beam of the VCSEL is directed by a mirror towards the input pad of the chip. The mirror is used to adjust the incidence angle. At the resonance wavelength, a fraction of the light is coupled into the waveguide and coupled out through the output pad. The emitted light is collected by a multi-mode fiber and detected by a photodiode. The signal can then be acquired for peak position detection.

3. Design considerations

3.1. Substrate

For highly sensitive sensor applications, the mechanical and chemical stability of the sensor chips is of great importance. For this reason, high quality glass substrates are clearly preferred over polymers. A tradeoff is the augmented fabrication cost due to the nanostructuring of the grating, as convenient replication techniques such as hot-embossing [14] can no longer be used.

3.2. Film thickness and sensitivity

The thickness of the waveguiding film h_f is an important design parameter for adjusting the sensitivity for different measurands. Depending on the application, a different film thickness has to be chosen for maximum sensitivity. In the present case, the sensor chips are optimized for protein adlayer thickness (h_l) variations. Table 1 gives an overview of the overall sensitivity $\delta\lambda/\delta M$ of the chips for different applications. The parameters used for the calculations were

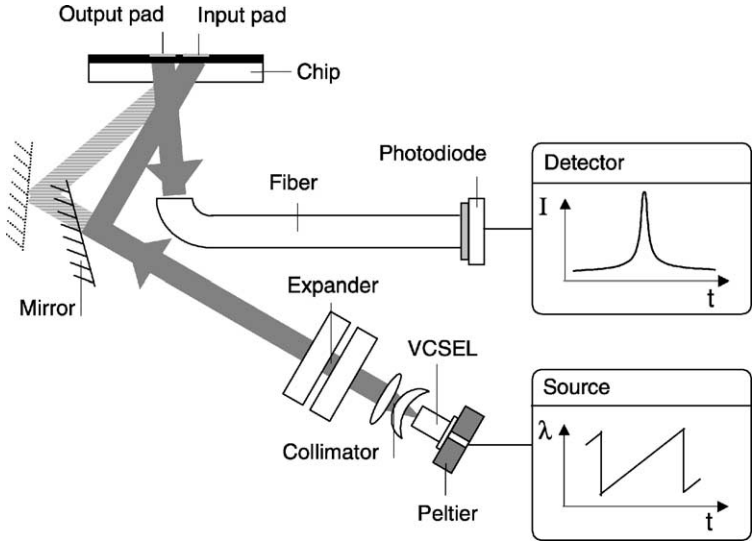

Fig. 3. WIOS optical scheme.

Table 1
Theoretical sensitivities for the WIOS system

Measurand	M	$\delta\lambda/\delta M$	Unit
Surface mass coverage	Γ	0.207	nm (mm^2/ng)
Adlayer thickness	h_l	0.122	nm/nm
Refractive index of adlayer	n_l	2.89	nm
Cover refractive index	n_c	72.8	nm

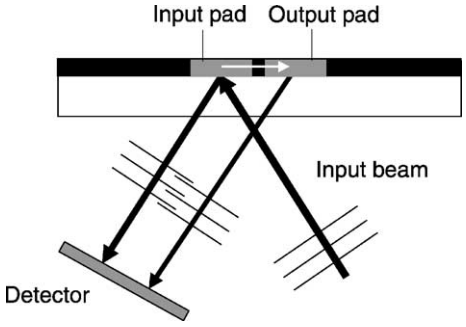

Fig. 4. Beam separation.

$n_c = 1.33$, $n_l = 1.45$, $h_l = 8.5$ nm, $n_f = 2.13$, $h_f = 150$ nm, $n_s = 1.52$, $\Lambda = 360$ nm, $\lambda = 763$ nm, TM_0. The surface mass coverage has been calculated as described in [19] with a surface coverage $\Gamma_m = 5$ ng/mm^2 corresponding to a saturated IgG monolayer of $h_l = 8.5$ nm adsorbed on a protein A layer.

3.3. Beam separation

If the input and output pads have the same coupling characteristics, reflections of the incident beam interfere with the outcoupled signal (Fig. 4). To prevent this, the in- and outcoupling angles have to be chosen differently. According to Eqs. (1) and (2), this can be achieved for instance by two gratings of different periods Λ_{in} and Λ_{out} (cf. Fig. 5a) or by two regions of same periods Λ but different film thicknesses $h_{f,in}$ $h_{f,out}$ [20] (cf. Fig. 5b). Both layouts have been fabricated, characterized and tested successfully in bio-chemical sensing applications.

3.4. On-chip referencing

In bio-chemical assays, a reference channel is used to separate specific from non-specific effects visible on the sensor response. These include changes of temperature and bulk refractive index, wavelength variations due to current instabilities of the laser diode, or non-specific binding [21,22]. The reference pad has the same characteristics as the sensing pad, but does not present the specificity of the sensing pad. During a measurement, the final signal is calculated by subtracting the reference peak position from the signal peak position.

Placing reference pads close to the sensing pads eliminates drift to a large extent, leading to much more relaxed stabilization criteria. Furthermore, it leads to a markedly increased signal to noise ratio, and therefore to a better detection limit.

4. Signal shape and calibration

4.1. Influence of parasitic reflections

The resonance curve as sensor output is disturbed in particular by parasitic reflections at the top and bottom substrate interfaces. The twice-reflected input beam is coupled into the waveguide with a phase ϕ_2 different from the phase ϕ_1 of the original wave, as can be seen in Fig. 6. As the phase difference $\Delta\phi = \phi_2 - \phi_1$ changes with the wavelength, this leads to a sinusoidal modulation of the resonance curve and to a deformation of the resonance peaks (Fig. 7).

The phase shift $\Delta\phi = \phi_2 - \phi_1$ is calculated by comparing the doubly reflected wave with the one incident at the same spot, having traveled a longer distance in the air:

$$\Delta\phi = \frac{4\pi h_s n_s}{\lambda}\left(\frac{1}{\cos\theta_s} - \sin^2(\theta_s)\right) + \varphi_{sf} + \varphi_{sa} \tag{7}$$

where n_s is the index of refraction of the substrate, λ the wavelength in air, φ_{sf} the Fresnel phase shift at the substrate-film boundary, φ_{sa} the Fresnel phase shift at the substrate-air boundary.

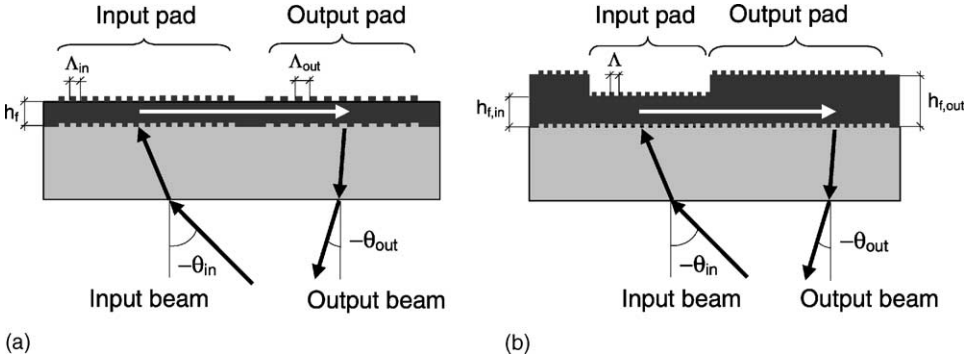

Fig. 5. (a) Cut through dual period sensor chip. (b) Cut through thickness-modulated sensor chip.

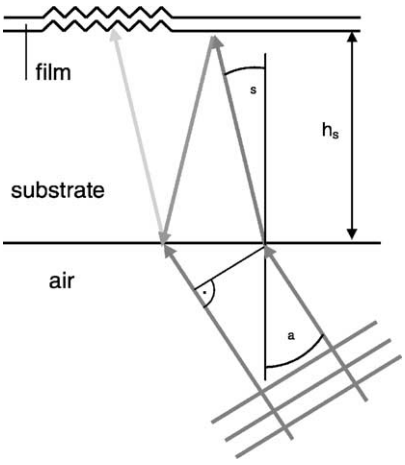

Fig. 6. Parasitic substrate reflections.

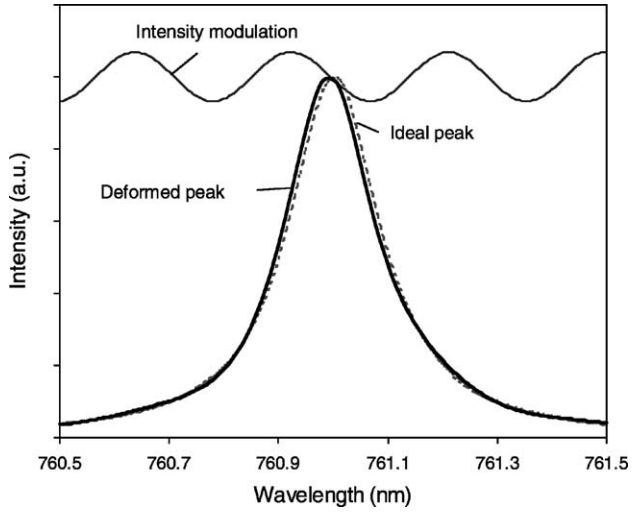

Fig. 7. Influence of parasitic substrate reflections on resonance peak shape.

The amplitude a_2 of the reflected wave is related to the amplitude a_1 of the original wave as

$$a_2 = a_1 r_{sf} r_{sa} \tag{8}$$

where r_{sf} the amplitude of the reflection coefficient at the substrate-film boundary, r_{sa} the amplitude of the reflection coefficient at the substrate-air boundary.

The intensity modulation I_{mod} of the signal corresponds to the interference term of the two waves. The impact on the signal peak shape is evaluated by expressing the modulation in terms of wavelength:

$$\frac{I_{bmod}}{I_1} = 2\frac{a_1 a_2}{a_1^2}\cos(\Delta\phi) = 2 r_{sf} r_{sa} \cos\left(\frac{\partial\Delta\phi}{\partial\lambda}\Delta\lambda\right) \tag{9}$$

where

$$\frac{\partial\Delta\phi}{\partial\lambda} = -\frac{4\pi h_s n_s}{\lambda^2}\left(\frac{1}{\cos\theta_s} - \sin^2(\theta_s)\right) + \frac{\partial\varphi_{sf}}{\partial\lambda} + \frac{\partial\varphi_{sa}}{\partial\lambda} \tag{10}$$

is the modulation frequency.

For a substrate of thickness $h_s = 0.7$ mm and refractive index $n_s = 1.52$, covered with a film of Ta_2O_5 ($h_f = 150$ nm, $n_f = 2.13$), with a grating structure of period $\Lambda = 360$ nm and illuminated with a laser source of wavelength $\lambda = 763$ nm, the resulting modulation has a relative intensity of 6.8% and a period of 0.29 nm (see Fig. 7).

4.2. Film thickness variations

If the film thickness is not constant over the whole input pad area, the resonance curve will get distorted. A different film height results in a different local propagation constant, and therefore to a different phase pickup between two adjacent grating lines. The peak broadens and its shape is altered depending on the film height profile. As the chips are optimized for maximum sensitivity to layer thickness changes, they are inevitably very sensitive to small film thickness variations.

This effect has been investigated in particular for thickness-modulated sensor chip layouts, where the etching step introduces height variations in the order of 0.5 nm. The resulting shoulder-like deformations are described in detail in [20].

4.3. Source characteristics

A current-tunable vertical cavity surface emitting laser (VCSEL) is chosen as the light source due to its compact size, low cost and high modulation frequency. The laser operates around a wavelength of 763 nm, with an accessible wavelength tuning range of about 2 nm. It has a nearly linear current–wavelength response, but output power depends also on the current. Fig. 8 shows the wavelength–power characteristics of the laser diode measured with a polarizer to select the mode polarization used for incoupling.

The resonance curve $\eta = f(\lambda)$ is deformed by the variation of the output power with the wavelength.

4.4. Calibration

The signal distortions and modulations mentioned under Sections 4.1–4.3 reduce the measurement accuracy if not properly taken into account.

In order to correct for the non-ideal peak shape, an in situ chip calibration procedure was developed.

As the incidence angle can be changed in the present set-up, the angle-resonance wavelength characteristic is recorded before the actual measurement. Therefore, the complete input angle range is scanned in small steps by the adjustable mirror (sketched in Fig. 3). For each step θ_k, several wavelength scans are averaged and the corresponding peak position $\lambda_{cal}(\theta_k)$ extracted. These data points are interpolated, resulting in the continuous curve $\lambda_{cal}(\theta)$ and its inverse relation $\theta_{cal}(\lambda)$. A linear fit is then applied to the measured points, representing the linearized characteristics $\lambda_{lin}(\theta)$.

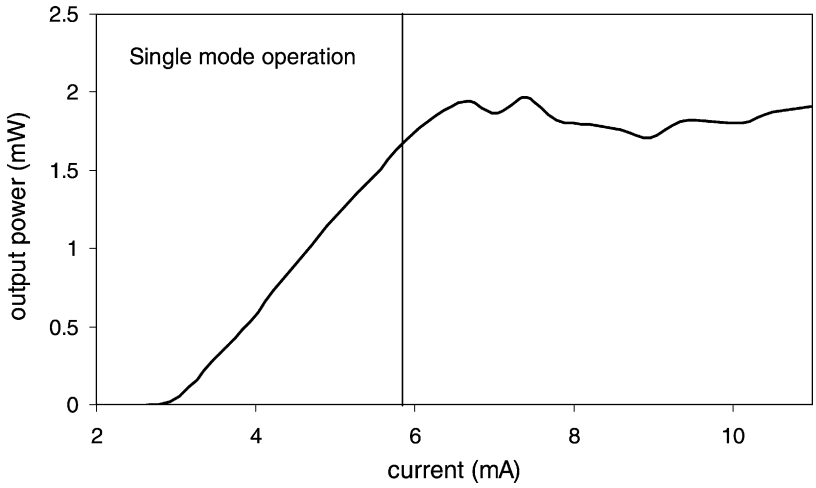

Fig. 8. VCSEL current–power characteristics.

During the actual measurement, the angle remains fixed and the wavelength scans are recorded over time. After the measurement, the measured peak positions λ_{meas} are corrected: $\lambda_{result} = \lambda_{lin}(\theta_{cal}(\lambda_{meas}))$.

For the calibration to work properly, it is necessary that both incoupling angle and effective refractive index follow a linear relation with the resonance wavelength. This condition is met inside the small measurement window.

5. Practical realization

5.1. Instrument

A compact WIOS instrument that has been realized is shown in Fig. 9. It allows the simultaneous readout of the resonance curves of four channels with a frequency of 300 Hz.

The following main components are visible on the photograph: (1) laser source, (2) beam expanding optics, (3) deflection mirror, (4) chip support with fluidic cell, and (5) array of plastic optical fibers.

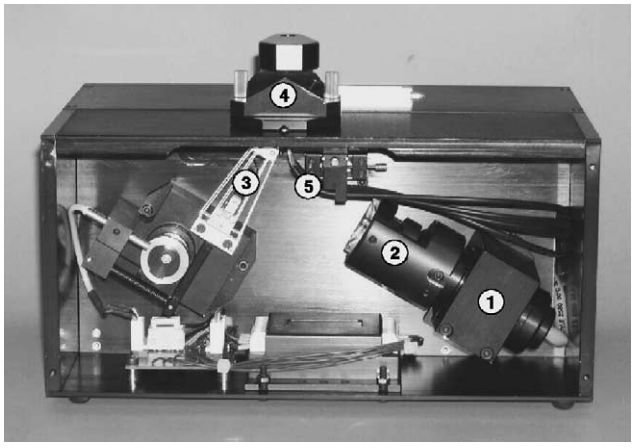

Fig. 9. Compact WIOS instrument. (1) Laser source, (2) beam expanding optics, (3) deflection mirror, (4) chip support with fluidic cell, and (5) array of plastic optical fibers.

As the light source, a VCSEL (Laser Components, SPECDILAS V-763-GMP) was used. The laser diode emits around a center wavelength of $\lambda = 763$ nm and has an accessible wavelength tuning range of about 2 nm. Its temperature is stabilized by a Peltier element, while the current is controlled by a custom electronic controller circuit. The deflection mirror has a range of 6° and is mounted on a motorized mechanical unit around the pivot axis located at the input grating. The output signal is detected by an array of photodiodes (OSRAM, SFH 206 K), amplified by a custom electronic circuit and acquired by a data acquisition board (National Instruments, PCI-6024E). The data is then treated on a personal computer.

5.2. Measurement procedure

Before starting the measurement, a proper angular working point is set. A reference cover medium (for example phosphate buffered saline solution PBS) is applied on the chip. The angular range is scanned by means of the motorized mirror. At the same time, calibration data (see Section 4.4) is collected. The mirror position then remains fixed in order to set the detected peak to a wanted starting position within the measurement range accessible by wavelength tuning. The actual measurement begins by removing the reference medium and applying the analyte. The peak positions of the reference and sensing pads are recorded over time. At the end of the measurement, the curves are corrected by applying the calibration and subtracting the reference from the sensing curve.

6. Sensor chips: fabrication

Two types of sensor chips have been realized as stated in Section 3.2. One layout consists of a waveguide structured

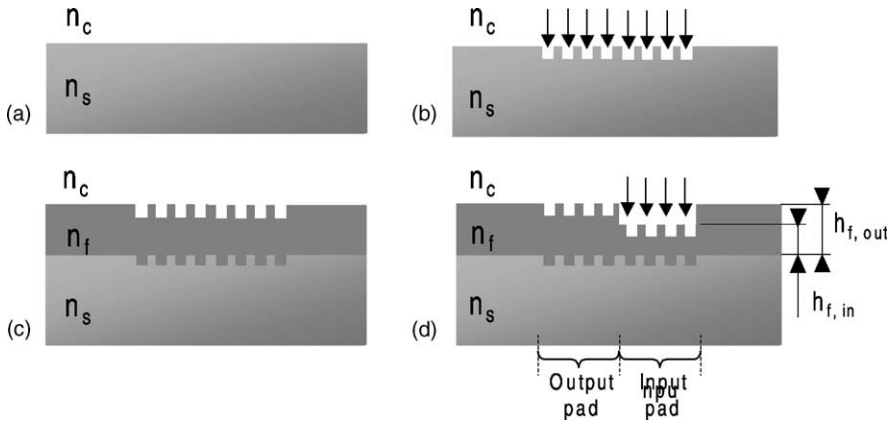

Fig. 10. Fabrication steps of depth-modulated sensor chips.

with two gratings of different period, defining the input and output pads. The other layout consists of a waveguide that is structured with a grating of uniform period, but presents two different film heights. The fabrication of the latter chip type is described in detail in the following.

For these so-called depth-modulated sensor chips, a fabrication process requiring only one holographic exposure has been established.

In Fig. 10, the main steps of the fabrication procedure are depicted. First, the surface of a 0.7 mm thick 4 in. AF45 glass wafer with a refractive index of $n_S = 1.52$ (at $\lambda = 632.8$ nm) was structured with a grating by holographic exposure (cf. Fig. 10a and b). In a second step, the grating structure was transferred into the substrate by dry etching as shown in Fig. 10b. During the etching, an aperture mask was applied to prevent gratings to be etched outside the input and output pad regions. The resulting grating had a period of $\Lambda = 360$ nm and a depth of $h_g = 13.2$ nm.

After removing the photoresist, the whole substrate was coated with a $h_{f,out} = 300$ nm thick Ta_2O_5 dielectric film using a low temperature DC magnetron sputtering process as shown in Fig. 10c. This process allows to fabricate thin, compact and homogeneous films with a high refractive index of $n_f = 2.10$ (at $\lambda = 632.8$ nm).

The structured substrate was coated with a second photoresist layer and the regions acting as input pads were exposed using an aperture mask. The film was then dry etched to a thickness of $h_{f,in} = 150$ nm as shown in Fig. 10d. While these regions acted as input pads, the regions remaining at the film thickness of $h_{f,out} = 300$ nm were used as output pads.

Finally the wafer was cut into single sensor chips of a size of 12.25 mm × 12.25 mm. Fig. 11 shows the picture of a sensor chip with six measuring channels. The dimensions of both the input and output pad were 0.8 mm × 1.0 mm. The triangular grating structure at the upper left corner is used as positioning reference.

A line-profile extracted from an AFM measurement of the transition region between input and output pad is plotted in Fig. 12. It shows that the transition width is less than one grating period. The measured step height was $\Delta h_f = h_{f,out} - h_{f,in} = 146.2$ nm. It can be seen on the graph that the grating height and profile is altered at the input pad region during the second etching step. The initial grating height of $h_g = 13.2$ nm is slightly reduced to $h_g = 12.7$ nm,

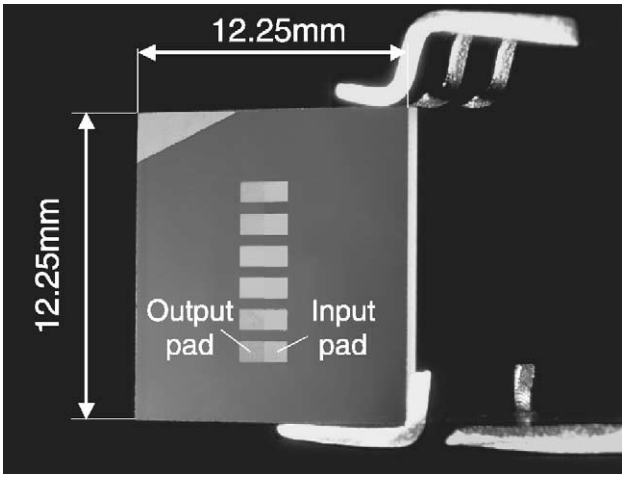

Fig. 11. Picture of the realized sensor chip with six channels.

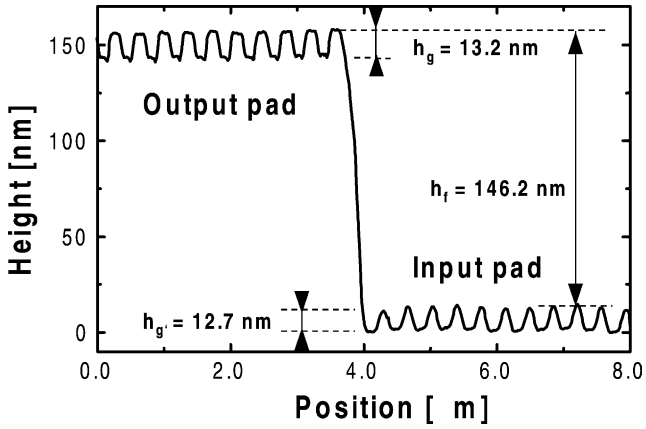

Fig. 12. AFM line profile of the transition between input and output region.

while the profile is changing from a trapezoidal to a smoother, more sinus like shape.

7. Applications

7.1. Bulk refractometry

Although the sensor chips were not optimized for refractometry of the cover medium (or bulk media in general), but for measuring thin adlayers formed near the waveguide's surface, refractometric measurements have been performed in order to evaluate the system sensitivity. For the series of measurements reported in Fig. 13, the following mixtures have been applied as the cover medium: 0.2, 1 and 5% glycerol in water, increasing the refractive index of the solutions by 0.00024, 0.0012 and 0.0058, respectively. The experiment was conducted by applying the solutions to the chip successively, always supplying water in between.

For this measurement, taking the raw data shown in Fig. 13 and determining the standard deviation of the signal over a time period of 1 min in a region with constant refractive index results in a value of 9.6×10^{-7} for the cover refractive index. This is the standard deviation for a single measuring pad, including drift and statistical fluctuations. If the signal of a reference pad is subtracted from the measuring pad signal (cf. Section 3.4), the standard deviation is reduced to 3.1×10^{-7}.

For obtaining a calibration, the measured shifts of the grating coupler resonance peak were compared with the shifts calculated using the known waveguide and grating parameters. The results confirmed the validity of all the system and chip parameters and were then used to obtain the relation between the resonance position and surface mass density of typical protein layers adsorbed on the waveguide grating.

7.2. Affinity measurements with small molecules

The most relevant applications for this system are in monitoring adsorption to and binding of molecules near the surface of the sensor chips. Many types of applications can be realized whenever a suitable recognition molecule–analyte couple exists. To demonstrate the performance of the system, the binding reaction of biotin on previously immobilized neutravidin was chosen. Using a double chamber fluid container, BSA and neutravidin were first adsorbed on two different channels of one waveguide chip, then biotin-5N-FITC with a molecular weight of 831 Da (cf. Fig. 14a) or pure biotin (cf. Fig. 14b) was supplied to both chambers simultaneously, the final concentration being 1 μg/ml. As the binding constant of biotin to neutravidin is high, the reaction takes place in a very short time (28 s) and drift due to the instrument or to the adsorbed layer is not significant. The binding of biotin can be clearly observed on the neutravidin coated pad whereas nothing occurs on the reference pad. The binding of biotin with a molecular weight of only 244 Da, one of the smallest molecules being of interest for biochemistry, is clearly demonstrated in Fig. 14b.

Examining the raw sensor signal data plotted in Fig. 14b yields a standard deviation of 0.009 peak position units for each pad, taken for 3 min in the steady regions, excluding the drift. The change of 0.613 units produced by adding the biotin solution is thus 67 times the standard deviation, corresponding to 22 times the detection limit. This indicates

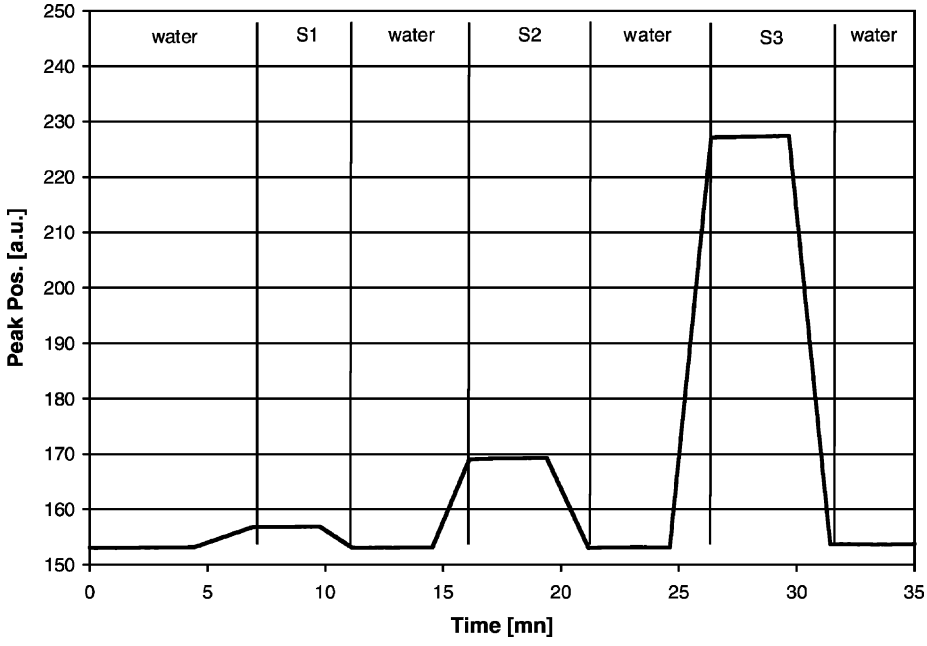

Fig. 13. Change of the resonance peak position for the three different refractive index solutions (water, *S*1: solution with $\Delta n = 0.00024$, *S*2 with $\Delta n = 0.0012$, and *S*3 with $\Delta n = 0.0058$).

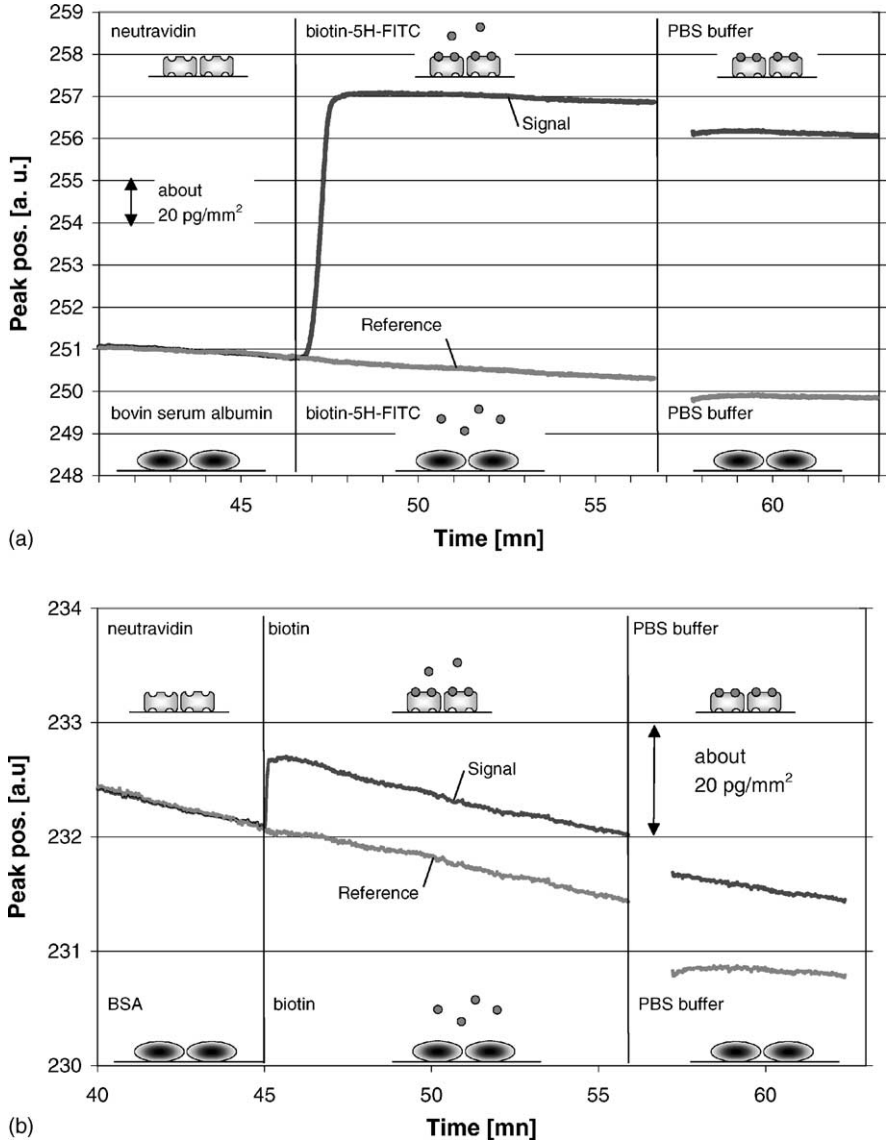

Fig. 14. Reaction of biotin-5H-FITC (a) and biotin (b) on adsorbed neutravidin (signal) and BSA (reference).

that the detection limit of the WIOS system is distinctly below 200 Da.

By making use of on-chip referencing (cf. Section 3.4), i.e. by subtracting the data of the reference from the signal curve (cf. Fig. 14b), the standard deviation is reduced to 0.005 peak position units, corresponding to about 100 fg/mm^2 and a detection limit of about 300 fg/mm^2. As in the case of bulk refractive index, this improvement is due to the fact that some signal disturbances originating for example from fluctuations in temperature and laser current, are affecting the signals from both pads in the same way.

7.3. Detection of large molecules at low concentration

Besides the detection of small molecules, the detection of larger molecules at low concentration is also an important feature for a biosensor. In order to show the performance of the WIOS approach for this type of application, we have chosen the reaction between anti-mouse antibody and mouse IgG. First, mouse IgG was immobilized on one grating pad using OptoDex® [23,24], i.e. a mixture of OptoDex® and mouse IgG (0.25 mg/ml each) were deposited on the pad. After drying, OptoDex® was activated with UV-light to induce the photobonding. The modified surfaces were then washed with phosphate buffered saline containing detergent (PBS/0.02% Tween 20) before being used in the system. A baseline was first established by supplying PBS–BSA buffer solution to the sensor cell, and then the buffer was replaced with solutions of anti-mouse IgG with decreasing concentrations of 10^{-10}, 10^{-9}, 10^{-8} M. The result of the measurement is shown in Fig. 15. It was made by pipetting without flow and without stirring. After 25 min of reaction the signal obtained with the lowest concentration is 0.26 units of peak shift, which is about five times the detection limit that can be

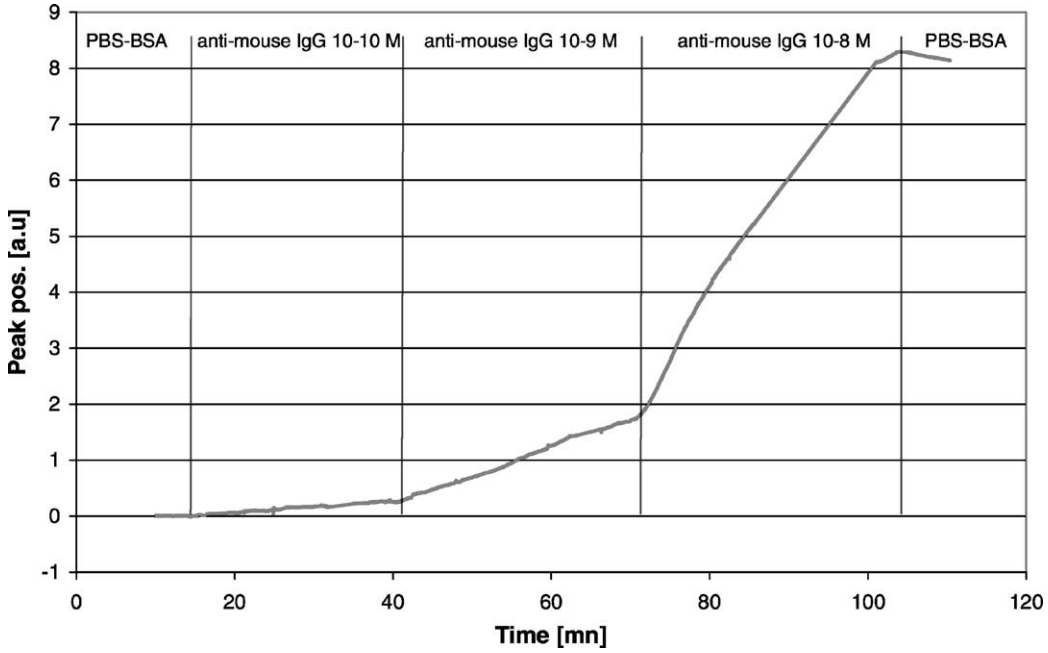

Fig. 15. Sensor signal upon the reaction of different concentrations of anti-mouse IgG supplied to the pad with immobilized mouse IgG (photobonded with OptoDex®). The reference was a bovine serum albumine coated pad.

obtained taking into account the drift of the instrument over the measurement time. A detection limit of 2×10^{-11} M can be expected for the same measurement conditions.

Considering the fact that the assay used was a direct immunoassay with photocoupled antigen, this is a very good result, especially if compared to sandwich assays. Further improvements can be achieved by making use of microfluidics and more sophisticated assays.

8. Conclusions

The WIOS bio-chemical sensor system based on wavelength interrogation of a waveguide grating has been presented. The label-free sensor combines fast readout with high sensitivity and accuracy. Some important design aspects have been pointed out, and sources of parasitic effects influencing the resonance peak shape have been identified and analyzed in detail. It has been shown that the use of a motorized deflection mirror allows calibrating the system in order to correct for these effects. The same mirror is used for setting the high-resolution measurement window within a large operating range.

The layout of two types of sensor chips has been presented together with fabrication details. The stability of the sensor chips has been enhanced by using glass rather than polymer substrates.

An excellent performance of the sensor has been demonstrated for bulk refractometry and affinity measurements. The bulk refractometric measurements show a detection limit of $<10^{-6}$. For detecting small molecules, a standard deviation in terms of mass coverage of 100 fg/mm^2 has been obtained, corresponding to a detection limit of 0.3 pg/mm^2. Furthermore, the very clear signal observed for biotin (244 Da) indicates a detection limit for the present WIOS system distinctly below 200 Da. For a direct immunoassay at low concentrations, a detection limit in the order of 10^{-11} M was estimated based on the results reported in this paper. These results show that the sensor is perfectly suited for application areas such as medical, food and environmental.

Acknowledgements

We gratefully acknowledge the help of F. Crevoisier, E. Bernard and R. Ischer with respect to performing experiments as well as for building the instruments, and B. Hitz from Unaxis with respect to chip fabrication. We also thank the Swiss CTI foundation for partly funding this project.

References

[1] M. Wiki, R.E. Kunz, Wavelength-interrogated optical sensors for biochemical applications, Opt. Lett. 25–27 (2000) 463–465.
[2] R. Horváth, J. Vörös, R. Graf, G. Fricsovszky, M. Textor, L.R. Lindvold, N.D. Spencer, E. Papp, Effect of patterns and inhomogeneities on the surface of waveguides used for optical waveguide lightmode spectroscopy applications, Appl. Phys. B 72 (2001) 441–447.
[3] K. Tiefenthaler, W. Lukosz, Sensitivity of grating couplers as integrated-optical chemical sensors, J. Opt. Soc. Am. B 6 (2) (1989) 209–220.
[4] J. Dübendorfer, R.E. Kunz, G. Jobst, I. Moser, G. Urban, Integrated optical pH sensor using replicated chirped grating coupler sensor chips, Sens. Actuators B 50–53 (1998) 210–219.

[5] R. Heidemann, R. Kooyman, J. Greve, Performance of a highly sensitive optical waveguide Mach-Zehnder interferometer immunosensor, Sens. Actuators B 10 (1993) 209–217.
[6] A. Brandenburg, R. Krauter, C. Künzel, M. Stefan, H. Schulte, Interferometric sensor for detection of surface-bound bioreactions, Appl. Opt.-OT 39(34) 6396.
[7] A. Ymeti, J.S. Kanger, R. Wijn, P.V. Lambeck, J. Greve, Development of a multichannel integrated interferometer immunosensor, Sens. Actuators B 83 (2002) 1–7.
[8] K. Nagata, H. Handa (Eds.), Real-Time Analysis of Biomolecular Interactions: Applications of 2000, Springer, Verlag, 2000.
[9] R. Cush, J.M. Cronin, W.J. Stewart, C.H. Maule, J. Molloy, N.J. Goddard, The resonant mirror: a novel optical biosensor for direct sensing of biomolecular interactions. Part 1. Principle of operation and associated instrumentation, Biosens. Bioelectron. 8 (1993) 347–353.
[10] R. Tünnemann, M. Mehlmann, R.D. Süssmuth, B. Bühler, S. Pelzer, W. Wohlleben, H.P. Fiedler, K.H. Wiesmüller, G. Gauglitz, G. Jung, Optical biosensors. monitoring studies of glycopeptide antibiotic fermentation using white light interference, Anal. Chem. 73 (2001) 4313–4318.
[11] G. Ladam, P. Schaad, J.C. Voegel, P. Schaaf, G. Decher, F. Cuisinier, In situ determination of the structural properties of initially deposited polyelectrolyte multilayers, Langmuir 16 (2000) 1249–1255.
[12] D.S. Ballantine, R.M. White, S.J. Martin, A.J. Ricco, E.T. Zellers, G.C. Frye, H. Wohltjen, Acoustic Wave Sensors: Theory, Design, and Physico-Chemical Application, Academic Press, San Diego, 1997.
[13] F. Höök, M. Rodahl, J. Vörös, R. Kurrat, P. Böni, J.J. Ramsden, M. Textor, N.D. Spencer, P. Tengvall, J. Gold, B. Kasemo, A comparative study of protein adsorption on titanium oxide surfaces using in situ ellipsometry, optical waveguide lightmode spectroscopy, and the quartz crystal microbalance/dissipation, Coll. Surf. B: Biointerf. 24 (2002) 155–170.
[14] R.E. Kunz, J. Edlinger, P. Sixt, M.T. Gale, Replicated chirped waveguide gratings for optical sensing applications, Sens. Actuators A 47 (1995) 482–486.
[15] R.E. Kunz, J. Duebendorfer, R.H. Morf, Finite grating depth effects for integrated optical sensors with high sensitivity, Biosens. Bioelectron. 11 (1996) 653–667.
[16] R.E. Kunz, L.U. Kempen, Miniature integrated optical sensors, Proc. SPIE 2068 (1994) 69–86.
[17] R.E. Kunz, J. Duebendorfer, Miniature integrated optical wavelength analyzer chip, Opt. Lett. 20 (1995) 2300–2303.
[18] R.E. Kunz, J. Edlinger, B.J. Curtis, M.T. Gale, L.U. Kempen, H. Rudigier, H. Schütz, Grating couplers in tapered waveguides for integrated optical sensing, Proc. SPIE 2068 (1994) 313–325.
[19] R.E. Kunz, G. Duveneck, M. Ehrat, Sensing pads for hybrid and monolithic integrated optical immunosensors, Proc. SPIE 2331 (1994) 2–17.
[20] K. Cottier, R.E. Kunz, G. Voirin, M. Wiki, Thickness-modulated waveguides for integrated optical sensing, Proc. SPIE 4616 (2002) 53–63.
[21] J. Dübendorfer, R.E. Kunz, Reference pads for miniature integrated optical sensors, Sens. Actuators B 38–39 (1997) 116–121.
[22] J. Dübendorfer, R.E. Kunz, E. Schürmann, G.L. Duveneck, M. Ehrat, Sensing and reference pads for integrated optical immunosensors, J. Biomed. Opt. 2 (1997) 391–400.
[23] I. Caelen, H. Gao, H. Sigrist, Protein density gradients on surfaces, Langmuir 18(7) 2463–2467.
[24] H. Sigrist, H. Gao, Biosensors @ CSEM, Chimia 53 (1999–2001) 81–86.

Biographies

Kaspar Cottier obtained the diploma (MSc degree) in microengineering with specialization in optics at the Swiss Federal Institute of Technology at Lausanne (EPFL) in February 2001. He is currently working on his PhD thesis at CSEM Neuchâtel (Switzerland) on integrated optical sensing, supervised by Rino E. Kunz.

Max Wiki studied physics from November 1991 until November 1996 at the Swiss Federal Institute of Technology (ETH) at Zurich. He finished his studies (MSc degree) with the master work entitled "Photorefractive Solitons in $KNbO_3$" at the Institute for Quantum Electronics of Prof. Dr. P. Günther. From 1996 until August 2000 he has worked at the CSEM Centre Suisse d'Electronique et de Microtechnique in Zurich on his PhD thesis on the topic of miniature integrated optical sensors systems based on disposable sensor chips, supervised by Dr. R.E. Kunz, Prof. Dr. R. Salathé (Swiss Federal Institute of Technology (EPFL) at Lausanne). In September 2000 he joined the R&D department of Unaxis Balzers Ltd. in Liechtenstein, where he is working on the design of BioChip substrates and the development of new technologies for the mass production of gratings and waveguides for biosensor applications.

Guy Voirin received his engineer diploma in physics in 1982 at ENSIEG in Grenoble, France. Then from 1982 to 1984 he carried out research on integrated optics on glass at the Institut Nationale Polytechnique de Grenoble where he received his PhD. After working at Radiall, Rosny-sous Bois, France, on the development of miniature fiber optical connector, he moved on in 1986 to CSEM, Neuchatel, Switzerland as a research and development engineer. He was involved in integrated optic technology on glass and on silicon and in the development of optical sensor for metrology. He is now involved in the development of optical biosensors. His expertise is on waveguide, waveguide sensor, grating couplers, interferometry, displacement measurement systems, evanescent wave sensing.

Hui Gao received her BS and MS degrees in chemistry from Nankai University, China, in 1985 and 1990, respectively. She received her PhD in biochemistry from the University of Bern, Switzerland, in 1994. Currently she is working in the field of surface bioengineering, which centre on photolink polymer-mediated immobilization of biomolecules on material surfaces and application in biosensor technology, biochips manufacturing and biomaterial.

Rino E. Kunz received his Matura (BA degree) from Gymnasium Winterthur, Switzerland, in 1965, and the diploma in physics (MS degree) from the Swiss Federal Institute of Technology (ETH) Zurich in 1971. Subsequently, he joined the Professur fuer Optik at ETH as a research and teaching assistant working in the field of physical optics. After having completed his PhD thesis on "Lifetimes of fluorescent molecules close to dielectric interfaces" in 1979, he enjoyed an IBM World Trade Postdoctoral Fellowship at IBM Research Laboratory in San Jose, California, USA, working on surface enhanced Raman scattering and elastic light scattering from metallic surfaces. From 1982 to 1987 he worked in the central R&D Optics Group of GRETAG Ltd., Regensdorf, in the fields of industrial laser materials processing, thin film design and photofinishing equipment design. He then joined the Optics Group at the Paul Scherrer Institute (PSI), Zurich, Switzerland, the emphasis of his work being on leading industry-related projects and PhD thesis supervising. Since 1997, his employment is with the Centre Suisse d'Electronique et de Microtechnique SA (CSEM), Zurich, holding a position of senior expert in the field of integrated optical sensing. Current research activities include integrated optical sensors, diffractive micro- and nano-relief structures, optoelectronic micro-systems and thin films. He teaches integrated optics at the Swiss Federal Institute of Technology Lausanne (EPFL) and is a member of the Optical Society of America (OSA), the Swiss Physical Society (SPG), the Swiss Society for Sensor Technology (SVS) and the Swiss Society for Optics and Microscopy (SSOM).